

Observation of anisotropic dispersive dark exciton dynamics in CrSBr

J. Sears,¹ W. He,¹ Y. Shen,¹ M. Lajer,¹ J. W. Villanova,² T. Berlijn,² F. Yakhou-Harris,³ N. B. Brookes,³ D. G. Chica,⁴ X. Roy,⁴ E. Baldini,⁵ V. Bisogni,⁶ S. Johnston,^{7,8} M. Mitrano,⁹ and M. P. M. Dean^{1,*}

¹*Department of Condensed Matter Physics and Materials Science,
Brookhaven National Laboratory, Upton, New York 11973, USA*

²*Center for Nanophase Materials Sciences, Oak Ridge National Laboratory, Oak Ridge, Tennessee 37831, USA*

³*European Synchrotron Radiation Facility (ESRF), B.P. 220, F-38043 Grenoble Cedex, France*

⁴*Chemistry Department, Columbia University, New York, NY 10027, USA*

⁵*Department of Physics, The University of Texas at Austin, Austin, Texas, USA, 78712*

⁶*National Synchrotron Light Source II, Brookhaven National Laboratory, Upton, New York 11973, USA*

⁷*Department of Physics and Astronomy, The University of Tennessee,
Knoxville, Tennessee 37966, USA*

⁸*Institute of Advanced Materials and Manufacturing, The University of Tennessee, Knoxville, Tennessee 37996, USA*

⁹*Department of Physics, Harvard University, Cambridge, Massachusetts 02138, USA*

(Dated: January 14, 2025)

Many-body excitons in CrSBr are attracting intense interest in view of their highly anisotropic magneto-optical coupling and their potential for novel optical interfaces within spintronic and magnonic devices. Characterizing the orbital character and propagation of these electronic excitations is crucial for understanding and controlling their behavior; however, this information is challenging to access. Ultra-high resolution resonant inelastic x-ray scattering is a momentum-resolved technique that can address these crucial questions. We present measurements collected at the Cr L_3 -edge which show a rich spectrum of excitations with a variety of spin-orbital characters. While most of these excitations appear to be localized, the dispersion of the lowest energy dark exciton indicates that it is able to propagate along both the a and b directions within the planes of the crystal. This two-dimensional character is surprising as it contrasts with electrical conductivity and the behavior of the bright exciton, both of which are strongly one-dimensional. The discovery of this propagating dark exciton highlights an unusual coexistence of one- and two-dimensional electronic behaviors in CrSBr.

Introduction.—The weak dielectric screening intrinsic to two-dimensional (2D) van der Waals (vdW) materials promotes the formation of excitons, quasiparticles consisting of a bound electron and hole pair. Excitons often dominate the optical response in these materials and have for this reason been intensively studied for potential optoelectronics applications [1–3]. Optically forbidden dark excitons can also strongly affect material properties [2, 4], and are of interest for coherence applications [5]. More recently, a variety of magnetic vdW materials have been reported [6, 7] with the potential to support excitons with intertwined electronic and magnetic properties. Resonant inelastic x-ray scattering (RIXS) is a versatile measurement technique that can detect these various types of electronic excitation, and provide information on their spin and orbital character not available from other techniques. RIXS also provides information about the exciton dispersion at nonzero momentum transfer, therefore probing the propagation of these excitations in the material. This type of in-depth characterization will be valuable for understanding and tuning functional excitons for incorporation into devices.

CrSBr is a vdW material that was recently found to be magnetic down to the monolayer limit [8], and also possesses several other desirable properties for embedding into electronic and magnetic devices. It is semiconducting, air-stable, and has a relatively high order-

ing temperature of $T_N \approx 132$ K [9–12]. Optical studies have identified a bright exciton at 1.37 eV, which shows a strong coupling with magnetism [13, 14]. This discovery has prompted a great deal of research investigating the potential for optical control and detection of electronic and magnetic quasiparticle excitations in CrSBr [14–16].

The bright exciton in CrSBr is understood to have a delocalized Wannier character and to arise from hybridization between the Cr $3d$ and S and Br p states [13]. We note that a number of optically bright features have been reported in the energy range of 1.3–1.4 eV, however these are thought to be a result of coupling either to phonons or polariton modes [17, 18]. The bare exciton energy has been found to be 1.37 eV in [18]. Photoluminescence measurements of the exciton show a striking anisotropy, with the exciton only visible when the light is polarized along the crystallographic b -axis [13, 19]. This is a consequence of the highly anisotropic band structure, which results in quasi-one-dimensional (1D) electronic conduction along the b axis and localization along the a axis. The 1D electronic behavior is counter-intuitive, but understandable through a careful inspection of the crystal structure [9] shown in Fig. 1(a), which is made up of apparently well-connected bilayers of CrS₄Br₂ octahedra. The electronic anisotropy is due to the Cr-ligand-Cr bond angles, which are $\sim 90^\circ$ along a and $\sim 180^\circ$ along b . The quasi-1D electronic conduction occurs along the nearly straight chains

of Cr and S running along the b direction [19, 20].

Here we present the first use of RIXS to determine the electronic character and propagation of excitons in CrSBr. We observed the previously reported bright exciton at 1.37 eV [18] and found that its momentum dependence is consistent with that expected for a 1D Wannier exciton. We also detected several previously unreported dark excitons at higher energies up to 2.5 eV. While the higher-energy excitations are non-dispersing indicating localized electronic excitations, the lowest-energy dark exciton at 1.45 eV shows more exotic behavior. This excitation shows a strong temperature dependence and an unusual 2D dispersion more consistent with local exchange hopping than with a Wannier exciton. The 2D nature of this propagating dark exciton contrasts with the generally 1D electronic behavior, highlighting the complex interplay between the 1D and 2D phenomena in CrSBr.

Methods.—Single crystals of CrSBr were synthesized and aligned as described in the Supplemental Material Sec. I [21]. Cr L_3 -edge RIXS measurements were performed at the ID32 beam line of the European Synchrotron Radiation Facility (ESRF) [22]. Unless otherwise specified, linear horizontal (π) incident x-ray polarization and a sample temperature of 30 K was used. The spectrometer was operated with a resolution of 28 meV for the reciprocal space maps and temperature dependence, and 53 meV for the energy maps.

The CrSBr data were interpreted using exact diagonalization (ED) methods based on the Kramers-Heisenberg equation [23–25]. Due to the strongly correlated nature of CrSBr, it is important to treat electron-electron interactions accurately. For these reasons, cluster approximations are particularly appropriate for modeling RIXS [23, 26]. We therefore use an Anderson impurity model (AIM) constructed from the cluster shown in Fig. 1(a) in which the Cr atoms are surrounded by 4 S and 2 Br atoms. As described in the Supplemental Material Sec. II [21], we first computed the electronic structure of CrSBr using density functional theory (DFT) and then performed a Wannier projection to generate a tight binding model with Cr $3d$, S $3p$, and Br $4p$ orbitals. Since only a subset of the p orbitals bond with Cr d states, the model can be implemented much more efficiently with essentially no loss in accuracy by representing the ligand states by 5 effective ligand orbitals that hybridize most strongly with the central Cr site [27]. The electronic Hamiltonian consists of two contributions, a four-fermion Coulomb interaction term and a two-fermion term with contributions from crystal field, hopping, and spin-orbit coupling. This model was solved using the Fortran ED solver provided by the EDRIXS package [24, 25].

Results and interpretation.—We used RIXS to measure the electronic excitations and their dynamics in CrSBr, with the incident photon energy tuned to the peak of the x-ray absorption spectroscopy (XAS) spectrum at the

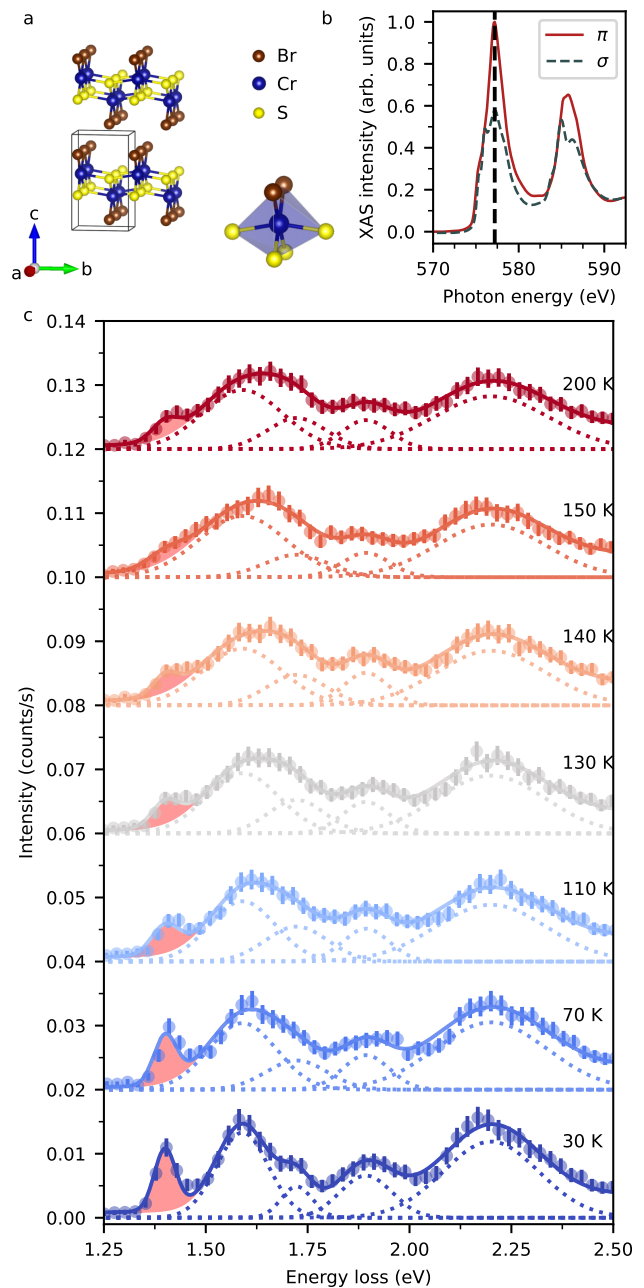


FIG. 1. Low-temperature emergence of excitons in CrSBr. (a) Crystal structure. The gray cuboid shows the unit cell and the translucent blue octahedron shows the Cr coordination. (b) X-ray absorption as a function of incident photon energy, showing peaks at the Cr L_3 and L_2 edges. The data was collected in the HOL plane, with an incident angle of approximately $\theta_i = 45^\circ$ and a scattering angle of $2\Theta \approx 90^\circ$. The dashed vertical line indicates the energy at which the RIXS spectra in (c) were collected. σ polarization indicates vertical linear polarization of the incoming beam along the sample b -axis, and π horizontal linear polarization in the sample $a-c$ plane. (c) RIXS spectra with varying temperature, collected at 577.2 eV (L_3 edge) at $\theta_i = 9.4^\circ$ and $2\Theta = 149^\circ$. A prominent excitation is visible at 1.4 eV and highlighted by the pink shading at low temperature, which becomes weaker and broader with increasing temperature. We found that the spectra can be accurately fit with five Gaussian functions with temperature-dependent widths and intensity, but with constant energies.

chromium L_3 edge. The XAS measurements collected with horizontal and vertical incident beam polarizations are shown in Fig. 1(b), with an energy range covering both the Cr L_3 and L_2 edges. These data were collected below the magnetic ordering temperature, and so show dichroism due to crystallographic and magnetic symmetry breaking.

The RIXS spectra collected at this energy show a number of features between 1.3 and 2.5 eV, as shown in Fig. 1(c), corresponding to different electronic excitations within the chromium d orbitals and hybridized ligand (S and Br) states. The temperature dependence is also shown in Fig. 1(c), from the base temperature of 30 K up to 200 K, well above the magnetic ordering temperature of 132 K. We find that the lowest energy (1.4 eV) excitation shows the largest change, nearly disappearing at the highest temperatures [28]. While the higher energy excitations become broader and weaker, they do not undergo the same loss in spectral weight. We note that the previously reported optically active exciton at 1.37 eV is not visible at this momentum transfer [$\vec{q} = (-0.29, 0, 0.28)$ reciprocal lattice units], but is apparent in the reciprocal space maps which we will discuss later.

In order to gain more insight into the nature of the electronic excitations, we simulated the RIXS spectra using a cluster model as described in the methods. RIXS has unique advantages for studying nominally optical dipole forbidden many body excitons, as it couples to them directly via a well known cross-section. This stands in contrast to optics, since the theoretical description of the optical cross-section for these modes is an area of active research [29]. In our model, the hopping parameters for the simulation were fixed using first-principles calculations. Since the effective octahedral crystal field parameter $10Dq$, Hund's coupling J_H , and the charge-transfer energy Δ , depend sensitively on electron-electron interactions, we follow typical analysis approaches for RIXS [27] and treated these as free parameters to fit the data, as described in the Supplemental Material Sec. III [21].

The results of this modeling are shown in Fig. 2(a), along with the measured spectra with horizontal and vertical linear polarization. We note first that the lowest energy excitations in the data were not well captured by the model, likely due to the limitations of the cluster approximation. The model can reproduce the peak positions at higher energies, with three features [labeled 1, 2, and 3 in Fig. 2(a)] at ~ 1.6 , 1.8, and 2.3 eV energy loss. The position of peak 1 was found to depend primarily on $10Dq$, and peak 2 on J_H . Once these two parameters were fixed, the value of Δ was adjusted to give the best match for the energy of peak 3.

The ground state of the model is high-spin $S \approx 3/2$ with strong ligand character and mixing between d^3 , $d^4\bar{L}$, and $d^5\bar{L}^2$ configurations, where \bar{L} denotes a ligand hole. The different excitations can be identified by computing the orbital occupancies, as well as the spin and or-

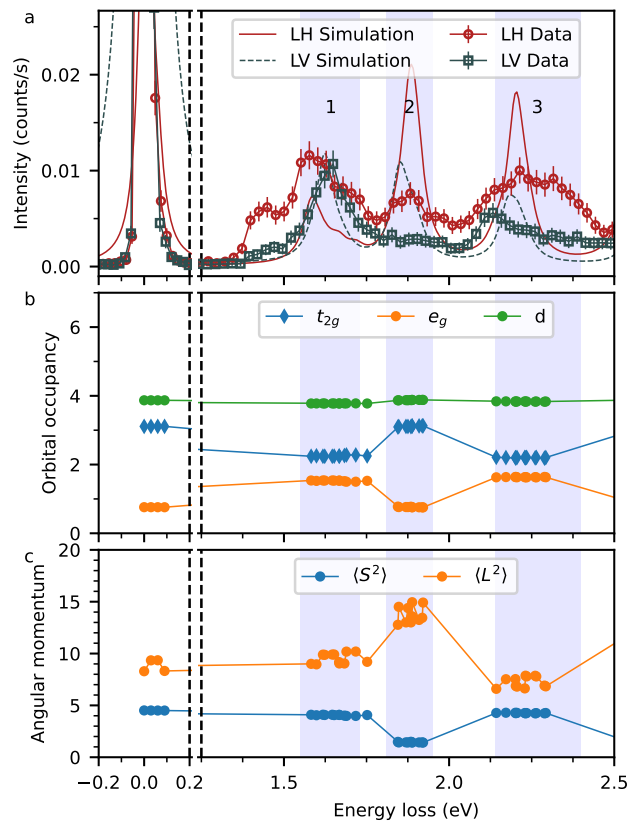


FIG. 2. Electronic character of the CrSBr excitons. (a) Low-temperature (30 K) RIXS spectra collected in the HOL plane at $\theta_i = 15^\circ$, $2\Theta = 90^\circ$ and 577.4 eV. (b),(c) Plot the orbital occupancies and magnetic expectation values of the excited states found extracted from our AIM calculations. We identify three manifolds of excitations: $t_{2g} \rightarrow e_g$ excitations below 1.75 eV, high spin-to-low-spin excitations from 1.75-2 eV, and a second manifold of $t_{2g} \rightarrow e_g$ excitations with reduced orbital angular momentum L above 2 eV.

bit magnetic moment expectation values for our AIM. These results are shown in Fig. 2(b) and (c), showing that the lowest energy manifold of excitations has a primarily $t_{2g} \rightarrow e_g$ character. This is indicated by the change in occupancy of the t_{2g} and e_g levels compared to the ground state, with no change in the spin or orbital moments. Feature 2 has instead a Hund's character, where t_{2g} occupancy remains the same but total spin is reduced. The highest energy manifold of excitations (peak 3) also has $t_{2g} \rightarrow e_g$ character, but with a reduced value of the total orbital angular momentum. This reflects the increased contribution of the $t_{2g} \rightarrow e_g$ transitions with higher Coulomb energy cost.

The modeling using AIM reproduces most of the major features in the RIXS spectrum, but does not correctly capture the lowest-energy excitations below 1.5 eV. This is likely due to the limitations of the cluster model, which cannot capture momentum-dependent or extended excitations. The 1.37 eV exciton reported in the optical mea-

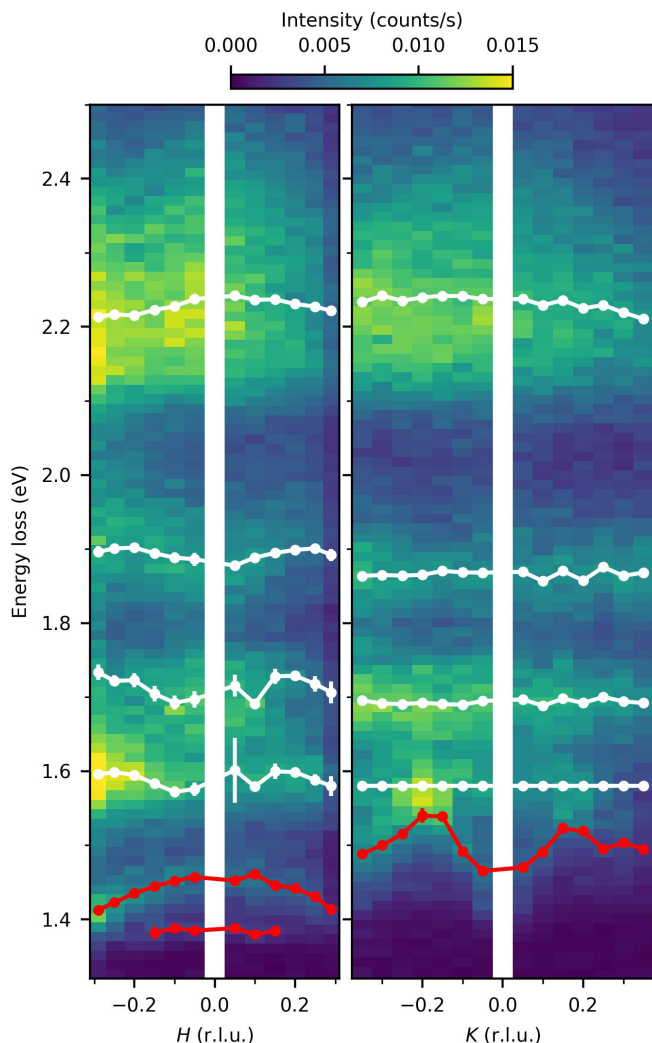


FIG. 3. Exciton propagation along the H and K directions of the Brillouin zone. The dispersion of the low (high) energy excitons, extracted from the fit, are shown in red (white), showing dispersive propagating behavior in one of the low-energy excitons.

measurements has been interpreted as being very delocalized (particularly along the crystallographic b -direction) and consequently too large to be accurately captured in the cluster model. As we will show later, the 1.4 eV excitation is strongly momentum dependent and not the type of localized excitation that can be fully captured within a small cluster. Despite these limitations, it seems probable that the 1.4 eV excitation, which exhibits the strongest temperature dependence, has the t_{2g} to e_g character of the lowest energy manifold in the model.

Due to the negligible momentum carried by optical light, optical spectroscopy — extensively applied to CrSBr in prior studies — cannot directly probe dispersion. In contrast, RIXS is used here to map the exciton dispersion as a function of the H and K recipro-

cal space directions (CrSBr is a highly 2D material, so no variation is expected in L [11]). The resulting reciprocal space maps are plotted in Fig. 3, and fit with Gaussian functions as described in Supplemental Material Sec. IV [21], evincing that the ~ 1.4 eV excitation is the only one to exhibit significant dispersion. This excitation also shows an intriguing asymmetry dispersing downwards along H and upwards along K . Despite the magnitude of electronic hopping along H and K differing by several orders of magnitude, the bandwidth of the exciton dispersion along H and K is of quite similar magnitude (~ 50 meV). This magnitude of dispersion is incompatible with a conventional particle-hole picture of the exciton, as this would require a far larger dispersive bandwidth along b due to the larger hopping in this direction, but is compatible with an exciton that moves via exchange processes. Although similar exchange bandwidths along H and K is superficially surprising in view of the very different hopping strengths in the two directions, it can be rationalized in view of bond-angle-dependent cancellation between different superexchange processes [30]. This type of cancellation is thought to be the mechanism behind the relatively isotropic magnon bandwidth [11].

Lastly, we observed an additional, weak low energy feature in the low momentum transfer region of the H direction reciprocal space map. This feature matches very well the 1.37 eV energy reported for the exciton in optical measurements [18]. The 1.37 eV feature is not seen in the K direction map, as expected for a band-edge excitation which would quickly disperse to higher energies in this direction due to the band anisotropy. It would then not be observable in our measurements since it would overlap with the higher energy localized excitations.

Conclusions.—Our RIXS measurements of electronic excitations in CrSBr allowed us to characterize the momentum dependence of the full complement of electronic excitations, including optically dark excitons not previously reported. The co-existence of 2D dark excitons and 1D bright excitons may open long-term routes to control the directionality of exciton transport by exciting CrSBr at different energies [31] and dark excitons offer possibilities for modifying the optical activity of these excitons in search of future coherence applications [2, 4, 5]. Comparing the measured spectra with the model results also allows us to determine the probable orbital and spin character of these excitons, providing a comprehensive characterization of the electronic excitations in this candidate functional material.

We detect the previously reported bright exciton at 1.37 eV, but also find a rich spectrum including a number of dark excitons at higher energies. The bright exciton shows the momentum dependence expected for a highly one-dimensional band-edge excitation, while most of the dark excitons do not show dispersion. However, the lowest energy dark exciton (1.5 eV at the Brillouin zone center and 1.45 eV at $\vec{q} = (-0.29, 0, 0.28)$) shows

more exotic behavior namely a strong temperature dependence and an anisotropic dispersion. This excitation disperses downwards along H and upwards along K , both with similar ~ 50 meV bandwidth. Such a dispersion is not compatible with a conventional Wannier exciton, but suggests that this excitation propagates via exchange processes.

Our simulations using a cluster model allow us to assign the character of the various observed excitons. We find that the lowest energy (< 1.8 eV) excitations involve excitation of t_{2g} electrons to the e_g levels. The Hund's coupling has a slightly higher energy scale, leading to a peak in the RIXS spectrum at 1.9 eV, where the excited state involves a spin flip of one of the t_{2g} electrons. While the substructure in the lowest energy manifold of excitations is not fully captured by model, it seems probable that these excitations are of $t_{2g} \rightarrow e_g$ character since the results of our modeling show that the Hund's coupling contributes at somewhat higher energy scales. We conclude that the anisotropic dispersing dark exciton we observe at 1.45 eV most likely has this orbital character and does not involve a spin flip. The discovery of this unusual exciton underlines the coexistence of 1D and 2D behavior in CrSBr.

Work at Brookhaven is supported by the Office of Basic Energy Sciences, Materials Sciences and Engineering Division, U.S. Department of Energy (DOE) under Contract No. DE-SC0012704. Work at the University of Tennessee (RIXS calculations and interpretation by model Hamiltonian calculations) was supported by the U.S. Department of Energy, Office of Science, Office of Basic Energy Sciences, under Award No. DE-SC0022311. E.B. was supported by the United States Army Research Office (W911NF-23-1-0394). This research used ESRF beam line ID32 under the proposals HC5030. Part of this research (T.B.) was conducted at the Center for Nanophase Materials Sciences, which is a DOE Office of Science User Facility. The work by J.W.V. is supported by the Quantum Science Center (QSC), a National Quantum Information Science Research Center of DOE. We also acknowledge resources made available through BNL/LDRD#19-013. This research used beamline 2-ID of the National Synchrotron Light Source II, a U.S. DOE Office of Science User Facility operated for the DOE Office of Science by Brookhaven National Laboratory under Contract No. DE-SC0012704. Crystal structures were rendered using VESTA [32].

* mdean@bnl.gov

- [1] G. Wang, A. Chernikov, M. M. Glazov, T. F. Heinz, X. Marie, T. Amand, and B. Urbaszek, Colloquium: Excitons in atomically thin transition metal dichalcogenides, *Rev. Mod. Phys.* **90**, 021001 (2018).
- [2] T. Mueller and E. Malic, Exciton physics and device application of two-dimensional transition metal dichalcogenide semiconductors, *npj 2D Materials and Applications* **2**, 29 (2018).
- [3] N. P. Wilson, W. Yao, J. Shan, and X. Xu, Excitons and emergent quantum phenomena in stacked 2d semiconductors, *Nature* **599**, 383 (2021).
- [4] M. R. Molas, C. Faugeras, A. O. Slobodeniuk, K. Nogajewski, M. Bartos, D. M. Basko, and M. Potemski, Brightening of dark excitons in monolayers of semiconducting transition metal dichalcogenides, *2D Materials* **4**, 021003 (2017).
- [5] J. Zhu, Y. Li, X. Lin, Y. Han, and K. Wu, Coherent phenomena and dynamics of lead halide perovskite nanocrystals for quantum information technologies, *Nature Materials* **23**, 1027 (2024).
- [6] K. S. Burch, D. Mandrus, and J.-G. Park, Magnetism in two-dimensional van der Waals materials, *Nature* **563**, 47 (2018).
- [7] Q. H. Wang, A. Bedoya-Pinto, M. Blei, A. H. Dismukes, A. Hamo, S. Jenkins, M. Koperski, Y. Liu, Q.-C. Sun, E. J. Telford, H. H. Kim, M. Augustin, U. Vool, J.-X. Yin, L. H. Li, A. Falin, C. R. Dean, F. Casanova, R. F. L. Evans, M. Chshiev, A. Mishchenko, C. Petrovic, R. He, L. Zhao, A. W. Tsun, B. D. Gerardot, M. Brotons-Gisbert, Z. Guguchia, X. Roy, S. Tongay, Z. Wang, M. Z. Hasan, J. Wrachtrup, A. Yacoby, A. Fert, S. Parkin, K. S. Novoselov, P. Dai, L. Balicas, and E. J. G. Santos, The magnetic genome of two-dimensional van der Waals materials, *ACS Nano* **16**, 6960 (2022).
- [8] K. Lee, A. H. Dismukes, E. J. Telford, R. A. Wisconsin, J. Wang, X. Xu, C. Nuckolls, C. R. Dean, X. Roy, and X. Zhu, Magnetic order and symmetry in the 2D semiconductor CrSBr, *Nano Letters* **21**, 3511 (2021).
- [9] O. Goser, W. Paul, and H. G. Kahle, Magnetic properties of CrSBr, *Journal of Magnetism and Magnetic Materials* **92**, 129 (1990).
- [10] E. J. Telford, A. H. Dismukes, K. Lee, M. Cheng, A. Wieteska, A. K. Bartholomew, Y.-S. Chen, X. Xu, A. N. Pasupathy, X. Zhu, C. R. Dean, and X. Roy, Layered antiferromagnetism induces large negative magnetoresistance in the van der Waals semiconductor CrSBr, *Advanced Materials* **32**, 2003240 (2020).
- [11] A. Scheie, M. Ziebel, D. G. Chica, Y. J. Bae, X. Wang, A. I. Kolesnikov, X. Zhu, and X. Roy, Spin waves and magnetic exchange Hamiltonian in CrSBr, *Advanced Science* **9**, 2202467 (2022).
- [12] M. E. Ziebel, M. L. Feuer, J. Cox, X. Zhu, C. R. Dean, and X. Roy, CrSBr: An air-stable, two-dimensional magnetic semiconductor, *Nano Letters* **24**, 4319 (2024).
- [13] N. P. Wilson, K. Lee, J. Cenker, K. Xie, A. H. Dismukes, E. J. Telford, J. Fonseca, S. Sivakumar, C. Dean, T. Cao, X. Roy, X. Xu, and X. Zhu, Interlayer electronic coupling on demand in a 2D magnetic semiconductor, *Nature Materials* **20**, 1657 (2021).
- [14] Y. J. Bae, J. Wang, A. Scheie, J. Xu, D. G. Chica, G. M. Diederich, J. Cenker, M. E. Ziebel, Y. Bai, H. Ren, C. R. Dean, M. Delor, X. Xu, X. Roy, A. D. Kent, and X. Zhu, Exciton-coupled coherent magnons in a 2D semiconductor, *Nature* **609**, 282 (2022).
- [15] G. M. Diederich, J. Cenker, Y. Ren, J. Fonseca, D. G. Chica, Y. J. Bae, X. Zhu, X. Roy, T. Cao, D. Xiao, and X. Xu, Tunable interaction between excitons and hybridized magnons in a layered semiconductor, *Nature Nanotechnology* **18**, 23 (2023).

- [16] F. Dirnberger, J. Quan, R. Bushati, G. M. Diederich, M. Florian, J. Klein, K. Mosina, Z. Sofer, X. Xu, A. Kamra, F. J. García-Vidal, A. Alù, and V. M. Menon, Magneto-optics in a van der Waals magnet tuned by self-hybridized polaritons, *Nature* **620**, 533 (2023).
- [17] K. Lin, X. Sun, F. Dirnberger, Y. Li, J. Qu, P. Wen, Z. Sofer, A. Söll, S. Winnerl, M. Helm, S. Zhou, Y. Dan, and S. Prucnal, Strong exciton–phonon coupling as a fingerprint of magnetic ordering in van der waals layered crsbr, *ACS Nano* **18**, 2898 (2024).
- [18] T. Wang, D. Zhang, S. Yang, Z. Lin, Q. Chen, J. Yang, Q. Gong, Z. Chen, Y. Ye, and W. Liu, Magnetically-dressed CrSBr exciton-polaritons in ultrastrong coupling regime, *Nat. Commun.* **14**, 5966 (2023).
- [19] F. Wu, I. Gutiérrez-Lezama, S. A. López-Paz, M. Gibertini, K. Watanabe, T. Taniguchi, F. O. von Rohr, N. Ubrig, and A. F. Morpurgo, Quasi-1D electronic transport in a 2D magnetic semiconductor, *Advanced Materials* **34**, 2109759 (2022).
- [20] J. Klein, B. Pingault, M. Florian, M.-C. Heißenbüttel, A. Steinhoff, Z. Song, K. Torres, F. Dirnberger, J. B. Curtis, M. Weile, A. Penn, T. Deilmann, R. Dana, R. Bushati, J. Quan, J. Luxa, Z. Sofer, A. Alù, V. M. Menon, U. Wurstbauer, M. Rohlfing, P. Narang, M. Lončar, and F. M. Ross, The bulk van der Waals layered magnet CrSBr is a quasi-1D material, *ACS Nano* **17**, 5316 (2023).
- [21] See Supplemental Material at [URL will be inserted by publisher] for details of the sample growth, first principles calculations, model parameters, and dispersion fitting, which also includes references [33–44].
- [22] N. Brookes, F. Yakhou-Harris, K. Kummer, A. Fondacaro, J. Cezar, D. Betto, E. Velez-Fort, A. Amorese, G. Ghiringhelli, L. Braicovich, R. Barrett, G. Berruyer, F. Cianciosi, L. Eybert, P. Marion, P. van der Linden, and L. Zhang, The beamline ID32 at the ESRF for soft x-ray high energy resolution resonant inelastic x-ray scattering and polarisation dependent x-ray absorption spectroscopy, *Nucl. Instrum. Methods Phys. Res. Sec. A* **903**, 175 (2018).
- [23] M. Mitrano, S. Johnston, Y.-J. Kim, and M. P. M. Dean, Exploring quantum materials with resonant inelastic x-ray scattering, *Phys. Rev. X* **14**, 040501 (2024).
- [24] Y. Wang, G. Fabbris, M. Dean, and G. Kotliar, EDRIXS: An open source toolkit for simulating spectra of resonant inelastic x-ray scattering, *Comput. Phys. Commun.* **243**, 151 (2019).
- [25] EDRIXS website, <https://github.com/NSLS-II/edrixs> (2024), accessed: 2021-09-27.
- [26] L. J. P. Ament, M. van Veenendaal, T. P. Devereaux, J. P. Hill, and J. van den Brink, Resonant inelastic x-ray scattering studies of elementary excitations, *Rev. Mod. Phys.* **83**, 705 (2011).
- [27] M. W. Haverkort, M. Zwierzycki, and O. K. Andersen, Multiplet ligand-field theory using Wannier orbitals, *Phys. Rev. B* **85**, 165113 (2012).
- [28] In the temperature dependence in Fig. 1(c), the data at 150 K shows a slightly less intense exciton than is expected within the overall trend. We believe this does not constitute a physically meaningful change.
- [29] S. G. Louie, Y.-H. Chan, F. H. da Jornada, Z. Li, and D. Y. Qiu, Discovering and understanding materials through computation, *Nat. Mater.* **20**, 728 (2021).
- [30] J. Kanamori, Superexchange interaction and symmetry properties of electron orbitals, *Journal of Physics and Chemistry of Solids* **10**, 87 (1959).
- [31] E. Malic, R. Perea-Causin, R. Rosati, D. Erckensten, and S. Brem, Exciton transport in atomically thin semiconductors, *Nature Communications* **14**, 3430 (2023).
- [32] K. Momma and F. Izumi, *VESTA3* for three-dimensional visualization of crystal, volumetric and morphology data, *Journal of Applied Crystallography* **44**, 1272 (2011).
- [33] A. Bocquet, T. Saitoh, T. Mizokawa, and A. Fujimori, Systematics in the electronic structure of 3d transition-metal compounds, *Solid State Communications* **83**, 11 (1992).
- [34] J. P. Perdew, K. Burke, and M. Ernzerhof, Generalized gradient approximation made simple, *Phys. Rev. Lett.* **77**, 3865 (1996).
- [35] G. Kresse and J. Furthmüller, Efficiency of ab-initio total energy calculations for metals and semiconductors using a plane-wave basis set, *Computational Materials Science* **6**, 15 (1996).
- [36] A. A. Mostofi, J. R. Yates, G. Pizzi, Y.-S. Lee, I. Souza, D. Vanderbilt, and N. Marzari, An updated version of Wannier90: A tool for obtaining maximally-localised Wannier functions, *Computer Physics Communications* **185**, 2309 (2014).
- [37] G. Kresse and J. Furthmüller, Efficient iterative schemes for ab initio total-energy calculations using a plane-wave basis set, *Phys. Rev. B* **54**, 11169 (1996).
- [38] N. Marzari and D. Vanderbilt, Maximally localized generalized Wannier functions for composite energy bands, *Phys. Rev. B* **56**, 12847 (1997).
- [39] W. He, Y. Shen, K. Wohlfeld, J. Sears, J. Li, J. Pelliari, M. Walicki, S. Johnston, E. Baldini, V. Bisogni, M. Mitrano, and M. P. M. Dean, Magnetically propagating Hund’s exciton in van der Waals antiferromagnet NiPS₃, *Nature Communications* **15**, 3496 (2024).
- [40] R. D. Cowan, *The theory of atomic structure and spectra*, 3 (Univ of California Press, 1981).
- [41] S. Feldkemper and W. Weber, Generalized calculation of magnetic coupling constants for Mott-Hubbard insulators: Application to ferromagnetic Cr compounds, *Phys. Rev. B* **57**, 7755 (1998).
- [42] I. Souza, N. Marzari, and D. Vanderbilt, Maximally localized Wannier functions for entangled energy bands, *Phys. Rev. B* **65**, 035109 (2001).
- [43] G. Kresse and D. Joubert, From ultrasoft pseudopotentials to the projector augmented-wave method, *Phys. Rev. B* **59**, 1758 (1999).
- [44] P. E. Blöchl, Projector augmented-wave method, *Phys. Rev. B* **50**, 17953 (1994).

Observation of anisotropic dispersive dark exciton dynamics in CrSBr

J. Sears,¹ W. He,¹ Y. Shen,¹ M. Lajer,¹ J. W. Villanova,² T. Berlijn,² F. Yakhou-Harris,³ N. B. Brookes,³ D. G. Chica,⁴ X. Roy,⁴ E. Baldini,⁵ V. Bisogni,⁶ S. Johnston,^{7,8} M. Mitrano,⁹ and M. P. M. Dean^{1,*}

¹*Department of Condensed Matter Physics and Materials Science,
Brookhaven National Laboratory, Upton, New York 11973, USA*

²*Center for Nanophase Materials Sciences, Oak Ridge National Laboratory, Oak Ridge, Tennessee 37831, USA*

³*European Synchrotron Radiation Facility (ESRF), B.P. 220, F-38043 Grenoble Cedex, France*

⁴*Chemistry Department, Columbia University, New York, NY 10027, USA*

⁵*Department of Physics, The University of Texas at Austin, Austin, Texas, USA, 78712*

⁶*National Synchrotron Light Source II, Brookhaven National Laboratory, Upton, New York 11973, USA*

⁷*Department of Physics and Astronomy, The University of Tennessee, Knoxville, Tennessee 37966, USA*

⁸*Institute of Advanced Materials and Manufacturing, The University of Tennessee, Knoxville, Tennessee 37996, USA*

⁹*Department of Physics, Harvard University, Cambridge, Massachusetts 02138, USA*

CONTENTS

I. Crystal growth of CrSBr	1
II. First principles calculations and Wannierization	1
III. Parameters for Anderson Impurity Model Calculation	2
IV. Exciton dispersion fitting	4
References	4

I. CRYSTAL GROWTH OF CrSBr

Single crystals of CrSBr were synthesized via chemical vapor transport [1]. A slightly off-stoichiometric amount of chromium powder, chromium(III) bromide chunks, and sulfur pieces were loaded into a 12.7 mm outer diameter and 10.5 mm inner diameter fused silica tube and sealed to a length of 20 cm under vacuum (~ 30 mtorr). The ampule was subjected to a temperature gradient of 950°C (source side) to 850°C (sink side) for 72 hours in a computer-controlled two-zone tube furnace. The crystals were washed using a Cr^{2+} aqueous solution, deionized water, toluene, and acetone, resulting in shiny black plate-like single crystals with the surface normal along the crystallographic c axis. The crystal morphology tends to be rectangular, with the larger dimension parallel to the a axis. The single crystal used for this measurement had dimensions 1 mm along the b direction and 4 mm along the a direction. The crystal orientation was verified by Laue and single crystal diffraction prior to the resonant inelastic x-ray scattering (RIXS) experiment.

II. FIRST PRINCIPLES CALCULATIONS AND WANNIERIZATION

To determine the hopping parameter for our model of CrSBr, we first computed the electronic structure of CrSBr using the density functional theory (DFT) code VASP [2, 3]. The calculations are performed within the Perdew-Burke-Ernzerhof generalized gradient approximation [4] for the exchange-correlation functional without spin-orbit coupling. We use projector augmented wave pseudopotentials [5, 6] with an energy cutoff of 450 eV and a $20 \times 14 \times 10$ Monkhorst-Pack k -point mesh. We constructed a tight-binding model using WANNIER90 [7–9] by performing a Wannier projection of Cr $3d$, S $3p$, and Br $4p$ orbitals without maximal localization; as these constitute an isolated manifold of bands, disentanglement is also unnecessary.

Figure S1 shows an excellent agreement between the DFT and Wannier function band structures.

* mdean@bnl.gov

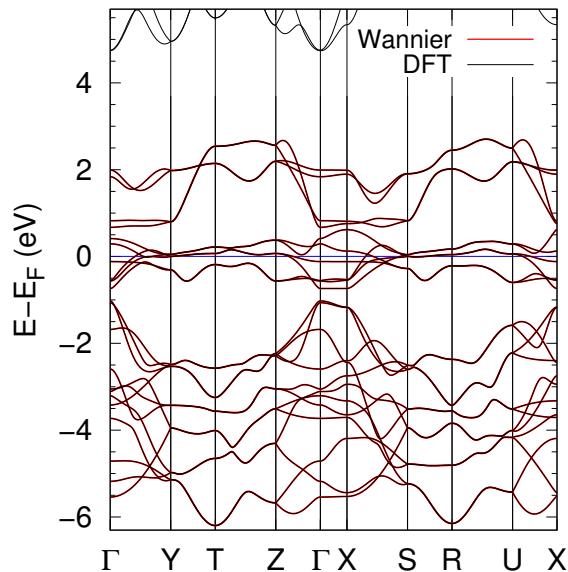


FIG. S1. Band structure of CrSBr without spin-orbit coupling. DFT calculated bands are in black, overlain on the Wannier projected bands in red, showing their total agreement.

III. PARAMETERS FOR ANDERSON IMPURITY MODEL CALCULATION

The RIXS cross section was modeled using an Anderson impurity model (AIM), which consists of a cluster made up of a single Cr atom and its surrounding ligand atoms (Br and S). The cluster includes the 10 Cr $3d$ spin-orbitals, as well as the 10 ligand molecular orbitals with the same symmetry [10] for a total of 20 orbitals occupied by 13 electrons. The Hamiltonian describing the cluster includes a four-fermion Coulomb term, and a two-fermion term which includes contributions from crystal field, hopping, spin-orbit, and magnetic field. The diagonalization of the Hamiltonian, and calculation of the cross sections were performed using the Fortran AIM solver provided by EDRIXS package [11, 12] following an approach similar to that used for NiPS₃ [13].

The four-fermion Coulomb term of the Hamiltonian includes interactions within the Cr $3d$ orbitals, as well as between the Cr $3d$ and Cr $2p$ orbitals in the intermediate state where a core hole is present. Coulomb interactions involving the ligand orbitals are expected to be relatively weak and so were not included. The Coulomb interactions for the Cr $3d$ orbitals can be described in terms of the Slater parameters F_{dd}^0 , F_{dd}^2 , and F_{dd}^4 , while those between the Cr $3d$ and Cr $2p$ are parametrized by F_{dp}^0 , F_{dp}^2 , G_{dp}^1 , G_{dp}^3 . Of these, F_{dd}^0 and F_{dp}^0 depend on the on-site Cr $3d$ Coulomb parameters U_{dd} and U_{dp} , which were set to typical values of 4 eV and 6 eV respectively [14, 15]. The results of the simulation do not depend strongly on the precise values chosen. The rest of the parameters (F_{dd}^2 , F_{dd}^4 , F_{dp}^2 , G_{dp}^1 , and G_{dp}^3) were set to their Hartree-Fock atomic values calculated by Cowan's code [16], scaled down to account for screening effects in the crystal. One scaling factor was used for the Cr $3d$ orbitals and one for the core-hole interactions, denoted k_{dd} and k_{dp} respectively. k_{dp} does not strongly affect the fit to the experimental data, and so is fixed to 0.5. This leaves the scaling parameter k_{dd} , which is proportional to the Hund's coupling, as the only free parameter in the Coulomb portion of the Hamiltonian. All of the Coulomb parameters are listed in Table S1.

The two-fermion term includes contributions from crystal field, hopping, spin-orbit coupling, and magnetic field. The crystal field and hopping terms are derived from the DFT calculation, and are shown in Eq. 1 as a 10×10 matrix. The order of the orbitals is as shown, listing first the Cr d orbitals and then the ligand L orbitals. The electronic structure calculation was not spin-resolved, and the same values were used for both spin-up and spin-down states in our EDRIXS calculation.

TABLE S1. Input parameters for the four-fermion term. All numbers are in units of eV, with the exception of k_{dd} and k_{dp} which are scaling parameters.

Initial State				
<i>d-d</i> Coulomb interactions				
U_{dd}	k_{dd}	F_{dd}^0	F_{dd}^2	F_{dd}^4
4	0.72	4.4	7.76	4.86

Intermediate State										
<i>d-d</i> Coulomb interactions					<i>d-p</i> Coulomb Interactions					
U_{dd}	k_{dd}	F_{dd}^0	F_{dd}^2	F_{dd}^4	U_{dp}	k_{dp}	F_{dp}^0	F_{dp}^2	G_{dp}^1	G_{dp}^3
4	0.72	4.43	8.35	5.23	6	0.5	6.22	3.26	2.39	1.36

$$\begin{pmatrix}
 d_{x^2-y^2} & d_{3z^2-r^2} & d_{xy} & d_{xz} & d_{yz} & L_{x^2-y^2} & L_{3z^2-r^2} & L_{xy} & L_{xz} & L_{yz} \\
 d_{x^2-y^2} & 3.201 & 0 & 0 & 0 & -2.426 & 0 & 0 & 0 & 0 \\
 d_{3z^2-r^2} & 0 & 3.227 & 0.0147 & 0 & 0 & -2.313 & -0.15 & 0 & 0 \\
 d_{xy} & 0 & 0.0147 & 2.662 & 0 & 0 & 0.159 & -1.49 & 0 & 0 \\
 d_{xz} & 0 & 0 & 0 & 2.733 & -0.041 & 0 & 0 & -1.383 & -0.068 \\
 d_{yz} & 0 & 0 & 0 & -0.041 & 2.733 & 0 & 0 & -0.068 & -1.383 \\
 L_{x^2-y^2} & -2.426 & 0 & 0 & 0 & 1.573 & 0 & 0 & 0 & 0 \\
 L_{3z^2-r^2} & 0 & -2.313 & 0.159 & 0 & 0 & 1.56 & 0.211 & 0 & 0 \\
 L_{xy} & 0 & -0.15 & -1.49 & 0 & 0 & 0.211 & -0.181 & 0 & 0 \\
 L_{xz} & 0 & 0 & 0 & -1.383 & -0.068 & 0 & 0 & 0.0096 & -0.061 \\
 L_{yz} & 0 & 0 & 0 & -0.068 & -1.383 & 0 & 0 & -0.061 & 0.0096
 \end{pmatrix} \quad (1)$$

The off-diagonal hopping terms in this matrix were not modified further, however it was necessary to adjust the diagonal (crystal field) terms as DFT includes Coulomb interactions at the mean-field level, so the on-site energies are subject to double-counting errors, which we need to avoid. In order to fit the data we therefore add a further splitting between the Cr e_g and t_{2g} orbitals, denoted $\Delta 10D_q$. The energy levels of the Cr and ligand states are also adjusted by adding an offset E_d to the diagonal terms for the metal orbitals and E_L to those for the ligand orbitals. These offsets were calculated using the EDRIXS functions `edrixs.utils.CT_imp_bath` and `edrixs.utils.CT_imp_bath_core_hole` with the arguments $U_{dd} = 4$ and $\delta = 0$. Adjusting this parameter δ has the effect of tuning the charge transfer energy Δ_{ct} , which is defined as the cost to move a hole from the metal d orbitals onto the lowest energy ligand orbital. We note that δ and Δ_{ct} are not related in a straightforward way. Δ_{ct} was calculated by diagonalizing the Hamiltonian with Cr-ligand hopping set to zero and then taking the energy difference between the d^3 and $d^4\bar{L}$ states (where \bar{L} denotes a ligand hole).

Spin-orbit coupling was also included in the two-fermion term, though this interaction is weak and does not strongly affect the results of the simulation. The spin-orbit parameters were therefore taken to be the atomic values. A small magnetic field of 15 meV was introduced to mimic the environment in the ferromagnetically ordered layers (the magnitude of the field was selected based on the magnon bandwidth reported in neutron measurements)[1]. As a result, there were two free parameters in the two-fermion term: the $10D_q$ splitting of the Cr d orbitals, and the splitting between the metal and the ligand orbitals parametrized as Δ_{ct} .

In summary, our calculation used three free parameters: an offset to the octahedral crystal field splitting $\Delta 10D_q$, the Coulomb scaling parameter k_{dd} (which scales with the Hund's coupling), and the charge transfer energy (Δ_{ct}). These

TABLE S2. Additional input parameters for two-fermion term. All numbers are in units of eV.

Charge transfer	Crystal field	Spin-orbit coupling			Magnetic field
Δ_{ct}	$\Delta 10D_q$	ζ_i	ζ_n	ζ_c	H
0.76	0.2	0.035	0.047	5.667	0.015

parameters (indicated in bold in Tables S1 and S2) were adjusted to best match the experimental RIXS spectra, while all other parameters were fixed to the specified values. Once the Hamiltonian was diagonalized, the RIXS and X-ray absorption spectrum (XAS) cross sections were calculated for the experimental geometry and polarization settings used for the measurements. An inverse core-hole lifetime broadening of $\Gamma_c = 0.6$ eV was used to compute the RIXS spectra. We used a final state inverse lifetime of $\Gamma_f = 0.03$ eV, which has the effect of broadening the spectra by a Lorentzian function with a full width half max of 0.03 eV.

IV. EXCITON DISPERSION FITTING

The spectra in Fig. 3 of the main text, were fit with either 5 or 6 Gaussian functions, depending on whether the low-energy exciton was visible. In the $0KL$ plane, the position and width of the excitation at ~ 1.6 eV were fixed to the fitted value from the scan at low K . The full width of the exciton at ~ 1.37 eV was fixed to the experimental resolution of 30 meV.

-
- [1] A. Scheie, M. Ziebel, D. G. Chica, Y. J. Bae, X. Wang, A. I. Kolesnikov, X. Zhu, and X. Roy, Spin waves and magnetic exchange Hamiltonian in CrSBr, *Advanced Science* **9**, 2202467 (2022).
 - [2] G. Kresse and J. Furthmüller, Efficient iterative schemes for ab initio total-energy calculations using a plane-wave basis set, *Phys. Rev. B* **54**, 11169 (1996).
 - [3] G. Kresse and J. Furthmüller, Efficiency of ab-initio total energy calculations for metals and semiconductors using a plane-wave basis set, *Computational Materials Science* **6**, 15 (1996).
 - [4] J. P. Perdew, K. Burke, and M. Ernzerhof, Generalized gradient approximation made simple, *Phys. Rev. Lett.* **77**, 3865 (1996).
 - [5] P. E. Blöchl, Projector augmented-wave method, *Phys. Rev. B* **50**, 17953 (1994).
 - [6] G. Kresse and D. Joubert, From ultrasoft pseudopotentials to the projector augmented-wave method, *Phys. Rev. B* **59**, 1758 (1999).
 - [7] A. A. Mostofi, J. R. Yates, G. Pizzi, Y.-S. Lee, I. Souza, D. Vanderbilt, and N. Marzari, An updated version of Wannier90: A tool for obtaining maximally-localised Wannier functions, *Computer Physics Communications* **185**, 2309 (2014).
 - [8] N. Marzari and D. Vanderbilt, Maximally localized generalized Wannier functions for composite energy bands, *Phys. Rev. B* **56**, 12847 (1997).
 - [9] I. Souza, N. Marzari, and D. Vanderbilt, Maximally localized Wannier functions for entangled energy bands, *Phys. Rev. B* **65**, 035109 (2001).
 - [10] M. W. Haverkort, M. Zwierzycki, and O. K. Andersen, Multiplet ligand-field theory using Wannier orbitals, *Phys. Rev. B* **85**, 165113 (2012).
 - [11] Y. Wang, G. Fabbris, M. Dean, and G. Kotliar, EDRIXS: An open source toolkit for simulating spectra of resonant inelastic x-ray scattering, *Comput. Phys. Commun.* **243**, 151 (2019).
 - [12] EDRIXS website, <https://github.com/NSLS-II/edrixs> (2024), accessed: 2021-09-27.
 - [13] W. He, Y. Shen, K. Wohlfeld, J. Sears, J. Li, J. Pellicciari, M. Walicki, S. Johnston, E. Baldini, V. Bisogni, M. Mitrano, and M. P. M. Dean, Magnetically propagating Hund's exciton in van der Waals antiferromagnet NiPS₃, *Nature Communications* **15**, 3496 (2024).
 - [14] A. Bocquet, T. Saitoh, T. Mizokawa, and A. Fujimori, Systematics in the electronic structure of 3d transition-metal compounds, *Solid State Communications* **83**, 11 (1992).
 - [15] S. Feldkemper and W. Weber, Generalized calculation of magnetic coupling constants for Mott-Hubbard insulators: Application to ferromagnetic Cr compounds, *Phys. Rev. B* **57**, 7755 (1998).
 - [16] R. D. Cowan, *The theory of atomic structure and spectra*, 3 (Univ of California Press, 1981).